

Optimisation of temporal averaging processes in PIV

Chaminda R. Samarage · Josie Carberry ·
Kerry Hourigan · Andreas Fouras

Received: 25 August 2010/Revised: 21 January 2011/Accepted: 18 March 2011/Published online: 1 April 2011
© Springer-Verlag 2011

Abstract A hybrid of correlation and vector averaging is introduced to capitalise on the advantages of each process. An extensive series of Monte Carlo simulations have been conducted to investigate hybrid averaging and evaluate it against both vector and correlation averaging. The simulations show that hybrid averaging improves the measurement accuracy over both correlation and vector averaging over a wide range of imaging conditions. The simulations are validated by applying hybrid averaging to experimental micro- and macro-flows. In pulsatile conditions, correlation averaging yields an averaged correlation function that is multi-modal, which can result in unpredictable measurements. A Monte Carlo simulation shows the benefits of hybrid averaging over correlation averaging in such conditions. This has been experimentally validated on the unsteady wake behind a shedding circular cylinder at $Re = 98$.

C. R. Samarage
Division of Biological Engineering,
Department of Mechanical & Aerospace Engineering,
Monash University, Melbourne, VIC 3800, Australia

J. Carberry
Fluids Laboratory for Aeronautical and Industrial Research
(FLAIR), Department of Mechanical & Aerospace
Engineering, Monash University, Melbourne,
VIC 3800, Australia

A. Fouras (✉)
Division of Biological Engineering, Monash University,
Melbourne, VIC 3800, Australia
e-mail: andreas.fouras@monash.edu

K. Hourigan
Division of Biological Engineering,
Fluids Laboratory for Aeronautical and Industrial
Research (FLAIR), Department of Mechanical & Aerospace
Engineering, Monash University, Melbourne,
VIC 3800, Australia

List of symbols

Roman

E_n	Image signal-to-noise ratio
M	Total number of image pairs within an image series
N	Number of image pairs in a correlation average
ppw	Particles per sampling window
Q	Number of image pairs in a vector average
r	Vector validation threshold
SNR	Signal-to-noise ratio
U	Magnitude of the velocity components, u and v
W	Sampling window size
V	Volumetric flow rate

Greek

ρ_1	Average number of particle image pairs in a sampling window
$\rho_{\text{effective}}$	Apparent number of particle image pairs
σ_{PIV}	Standard deviation of the vector error in pixels
μ_{PIV}	Mean of the vector error in pixels

1 Introduction

Significant improvements in the measurement accuracy and reliability of PIV have continued over the last two decades (Adrian 2005). Typical sources of PIV measurement error include correlation errors from inadequate seeding, loss of image pairs and inadequate particle image pairs (Keane and Adrian 1990, 1992), false correlations from unmatched particle pairs (Westerweel 1997), peak finding schemes (Lourenco and Krothapalli 1995; Huang et al. 1997; Roesgen 2003), velocity gradients (Keane and Adrian 1990) and non-uniform image seeding (Westerweel 1997). Recent advances in studying flow within

microscopic devices using microscopic particle image velocimetry (μ PIV) (Santiago et al. 1998; Meinhart et al. 1999) have emphasised the importance of additional sources of errors caused by out-of-focus particles (Olsen and Adrian 2000), the depth of correlation (Fouras et al. 2009) and Brownian motion (Olsen and Adrian 2000). Application of μ PIV (Nesbitt et al. 2009) and X-ray PIV (Fouras et al. 2007; Dubsky et al. 2010) to biomedical flows have gained popularity over the past decade. However, the high background image noise inherent in biomedical images reduces the precision of μ PIV measurements (Tiang and Qui 2002).

Image noise contributes to noisy artefacts in the cross-correlation map, and the exact displacement information is obscured. The displacement is measured by determining the integer location of the maximum signal (peak detection) and interpolating within the neighbouring correlation values to estimate the exact location of the signal (peak interpolation) with sub-pixel accuracy (Lourenco and Krothapalli 1995; Willert and Gharib 1991). In cases of very high noise in the cross-correlation map, the displacement peak is hidden amongst random noise peaks (Keane and Adrian 1992; Meinhart et al. 2000). In such cases, PIV interrogation is likely to return a random value – or *outlier* (Willert and Gharib 1991). Currently, a popular approach to reduce the effects of outliers is to use vector validation algorithms (Westerweel and Scarano 2005). Vector validation algorithms, however, rely on neighbouring vectors for validation, a process that may be compromised in cases with high correlation noise. Furthermore, vectors are validated based on a detection threshold addressing only obvious deviations, such as peak detection errors, while the vector errors on a sub-pixel level (i.e. peak interpolation errors) are neglected. In cases where time-averaged measurements are of importance, the effects of outliers may be diminished by temporal averaging of the vectors.

An obvious approach to reduce correlation errors is to improve the signal strength of the cross-correlation peak. Correlation-based correction (Hart 2000) involves multiplication of the correlation maps to filter out the noise anomalies. This technique however can also remove the maximum displacement signal in a noisy correlation map and proves ineffective for applications involving high image noise. Correlation averaging (sometimes referred to as ensemble averaging) (Meinhart et al. 2000) was originally developed to reduce the effects of Brownian motion, low image seeding and low image quality (Wereley and Meinhart 2010). The process has proven to be more robust than traditional processes such as vector averaging and image averaging (Meinhart et al. 2000). Correlation averaging has gained popularity over the years and is the most commonly used technique for studying micro-scale flows

(Santiago et al. 1998; Wereley and Meinhart 2010) as well as macro-scale applications (Fouras et al. 2008). Correlation averaging has been used for medical applications (Nesbitt et al. 2009; Irvine et al. 2008; Poelma et al. 2010) as well as studying dispersed two-phase flows (Delnoji et al. 1999) and PIV evaluation at a single pixel (Westerweel et al. 2004). Recently, correlation averaging has been used to improve the robustness of spatially adaptive non-isotropic algorithms (Theunissen et al. 2007, 2010). Averaging the cross-correlation map spatially or temporally, greatly improves the signal-to-noise ratio of the cross-correlation and enhances peak detection (Meinhart et al. 2000; Westerweel 2000; Wereley and Meinhart 2010).

Image averaging reduces the signal-to-noise ratio of the image and introduces noise to the cross-correlation map (Meinhart et al. 2000; Wereley and Meinhart 2010). Another image-based technique is image overlapping (Nguyen et al. 2010), which reduces the effect of out-of-focus particles in μ PIV images by overlapping the maximum pixel intensities in an image pair on to a single image pair. The technique is based on the work of Wereley et al. (2002), which was initially intended as a technique to increase the seeding density in μ PIV images.

A discussion of the most relevant temporal averaging processes in PIV and their respective error reduction schemes is presented in Sect. 2. At least one study has examined correlation averaging (Westerweel et al. 2004); however, a study of both correlation and vector averaging to further optimise PIV time-averaging processes has not been conducted. The authors propose that noise in the cross-correlation map leads to measurement errors through two processes: errors through peak detection and errors through peak interpolation. Correlation averaging improves the signal-to-noise ratio (SNR) of the cross-correlation map (Meinhart et al. 2000; Wereley and Meinhart 2010) and enhances peak detection. However, a common misconception is that correlation averaging optimises peak interpolation errors. The advantages and disadvantages of both correlation averaging and vector averaging are discussed in Sect. 2. In Sect. 3, a novel time-averaging algorithm is introduced that utilises current techniques to optimise the two different error processes. A Monte Carlo simulation utilising synthetic images is conducted to evaluate the new process for steady flow conditions. Recommendations for optimising time-averaging processes under steady conditions are made in Sect. 4. In Sect. 5, these simulations are validated by applying the hybrid averaging process to μ PIV data as well as macro-PIV data. A Monte Carlo simulation is conducted to test existing time-averaging processes as well as the hybrid averaging method under pulsatile flow conditions. To validate the synthetic

simulation, the novel process is applied to experimental flow behind a circular cylinder.

2 Background

2.1 Vector averaging

In vector averaging, instantaneous measurements are temporally averaged to yield an averaged displacement vector field (Landreth and Adrian 1990) (Fig. 1a). Since the decrease in the standard deviation of the measurements (σ_{PIV}) is related to the number of measurements averaged, Q , as shown in Eq. 1, vector averaging reduces the effects of interpolation errors on time-averaged measurements (Fig. 2a).

$$\sigma_{PIV} \propto \frac{1}{\sqrt{Q}} \quad (1)$$

Validating vectors (Westerweel and Scarano 2005) with respect to the neighbouring vectors can easily detect the most obvious of measurement deviations; however, the more subtle measurement errors at a sub-pixel level may not be identified. Exclusion of outliers from the vector average improves the accuracy of the vector averaging algorithm, while small errors do not significantly affect the time-averaged measurement. Outliers are statistically random in nature, and the probability distribution of these vectors, illustrated in Fig. 2b, has a mean of 0 px, and a high standard deviation that is a function of sampling domain geometry (Westerweel 1994). Inclusion of outliers in the vector average therefore introduces a measurement bias towards a mean of 0, while the standard deviation of the measurement increases, as illustrated in Fig. 2b.

A more recent and popular technique for obtaining time-averaged measurements is correlation averaging (or ensemble averaging) (Meinhart et al. 2000). Figure 1b shows a graphical representation of this process. It is recommended that the keen reader refer to Meinhart et al. (2000), for a detailed description of the algorithm.

Keane and Adrian (1992) showed that the amplitude of the averaged cross-correlation map is a function of the in-plane and out-of-plane loss-of-correlation and the image density (number of particle image pairs in a sampling window). Their study (Keane and Adrian 1992) recommended an image seeding density of at least 5–7 particle image pairs in a sampling window (ppw) to yield a cross-correlation map with sufficient signal strength for satisfactory peak detection probability. It was later confirmed that image seeding higher than 5 ppw produced little improvement in the PIV displacement error and that for these high seeding levels, the probability of detecting the

maximum correlation signal is a function of image seeding density (Westerweel 2000).

2.2 Correlation averaging

A Monte Carlo simulation using synthetic images was conducted to test the measurement accuracy of the correlation averaging technique as a function of seeding density and image noise. Since all parameters used for synthetic image generation, including the exact flow details, are known, the errors arising from the processing technique can be determined. Synthetic image series of resolution $1,024 \times 1,024$ px² were generated for different flow cases, with the parameters as shown in Table 1. The PIV data set used comprises of 1,024 image pairs.

Results for all flow cases were similar, and therefore, for clarity, only the case for Taylor vortices (Table 1: A) will be presented and discussed. For a given pair of images, the average number of particle image pairs in a sampling window is defined as the instantaneous seeding density, ρ_1 . The effective seeding density, $\rho_{\text{effective}}$, is the apparent number of particle image pairs per window after N number of correlation averages:

$$\rho_{\text{effective}} = \rho_1 \times N \quad (2)$$

White noise was added to the images by generating a random number with a Gaussian distribution of standard deviation, $\sigma = E_n\%$ of the maximum pixel intensity. The particle images have a Gaussian shape with a radius of 2.1 px to reduce the effect of precision errors governed by the particle image diameter (Willert 1996). The particle image diameter is defined as the full-width-half-max of the Gaussian function used to generate the particle image. The samples of the images (grey values of the pixels) are sampled at the pixel centre position, i.e. a pixel fill factor of 0. The sampling window size used was 32×32 px². The common 3-point parabolic fit (Willert and Gharib 1991) is used to determine the displacement with sub-pixel accuracy. The instantaneous seeding density, ρ_1 , is varied from $\rho_1 = \frac{1}{16}$ ppw to $\rho_1 = 16$ ppw (Fig. 3a) and the image noise ratio E_n is varied from $E_n = 0.05\%$ to $E_n = 70\%$ (Fig. 3b). Data for noise levels of above $E_n = 50\%$ are not discussed as the effect of the noise on the correlation map causes the peak detection to be random and produces inconclusive results. At extremely high noise levels, the reader is referred to literature discussing noise reduction (Westerweel 1997; Nguyen et al. 2010; Wereley et al. 2002). The number of instantaneous cross-correlation maps, N , included in a correlation average is varied from $N = 1$ to $N = 1,024$ and statistics for the error are determined.

Figure 3a shows the standard deviation of the PIV error, σ_{PIV} , as a function of $\rho_{\text{effective}}$ for a range of instantaneous

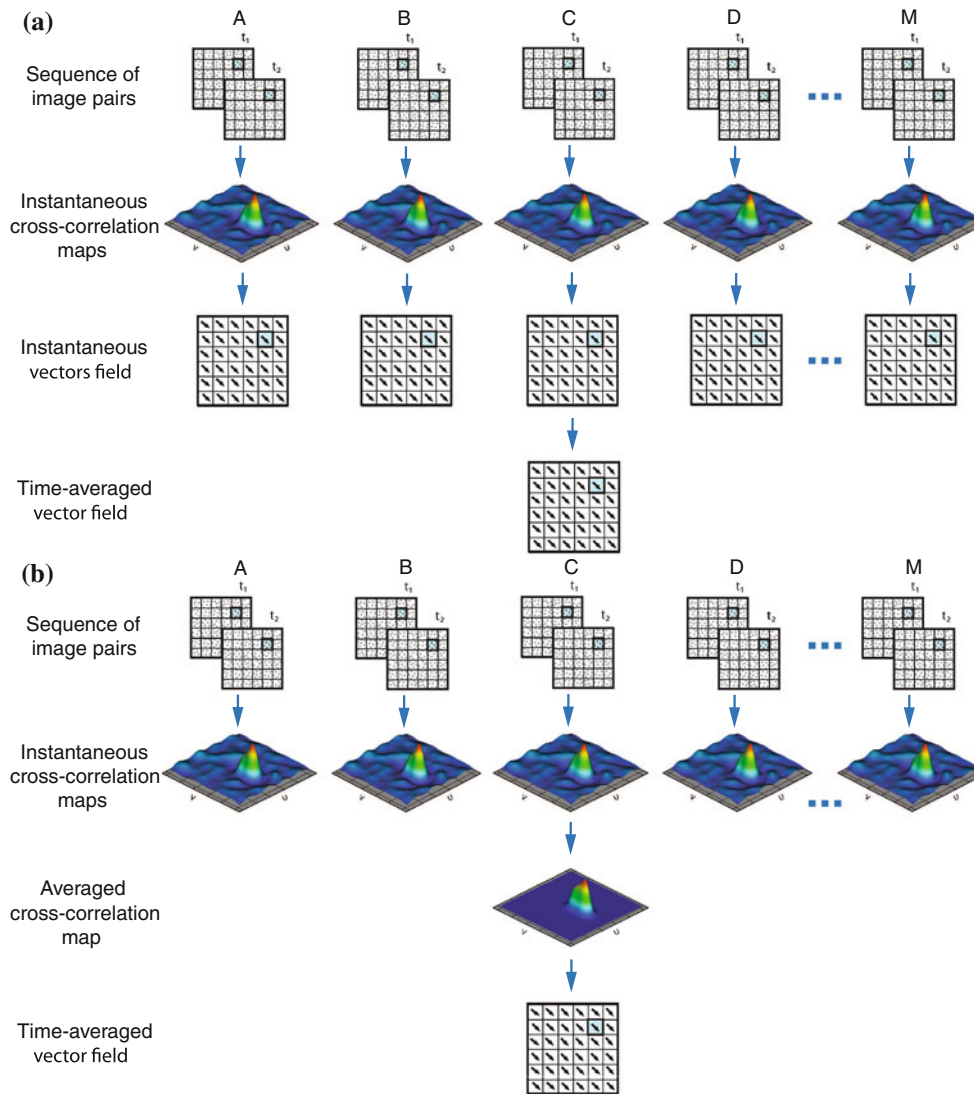


Fig. 1 Schematic diagrams of current averaging processes. **(a)** Vector averaging: instantaneous vectors are evaluated from instantaneous correlation maps and then averaged to yield a time-averaged displacement

vector. **(b)** Correlation averaging: instantaneous cross-correlation maps are averaged to yield a single correlation map. This single cross-correlation map is interrogated to obtain a time-averaged displacement vector

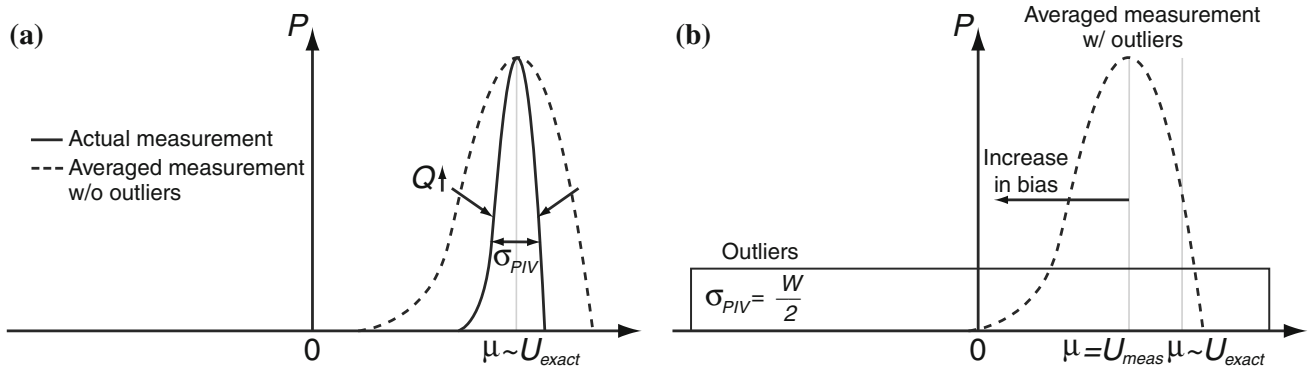


Fig. 2 Probability density functions (PDF) for instantaneous and vector-averaged velocity measurements. **(a)** Vector averaging reduces the PIV error with $1/\sqrt{Q}$. Increasing Q reduces the standard deviation of the measurement velocity PDF, and the mean measurement converges towards the exact displacement of the particles. **(b)** Outliers

have a PDF with a mean of 0 and a large standard deviation, which is a function of the sampling window size, W . As outliers are included in a vector average, the averaged measurement is biased towards a mean of 0 and the standard deviation is increased

Table 1 Details of flow cases studied

Case	Flow type	Flow conditions
A	Taylor vortices	$u, v = -12$ to 12 px
B	Constant flow	$u = 5$ px, $v = 0$ px
C	Low spatial gradient flow	$u, v = 4$ to 5 px
D	Pulsatile flow	$u, v = 5\cos(\omega t)$ px
E	Micro-channel stenosis model	$V = 0.48$ ml/min
F	Wake behind a cylinder	$Re = 66$ and $Re = 99$ (Ng et al. 2011)

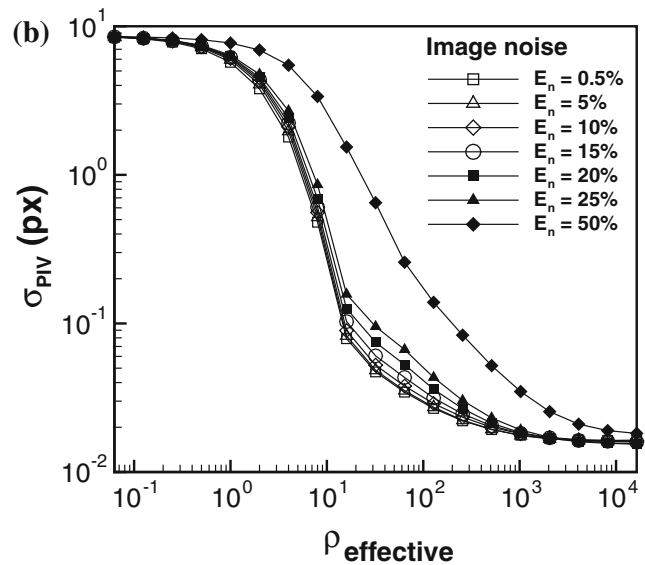
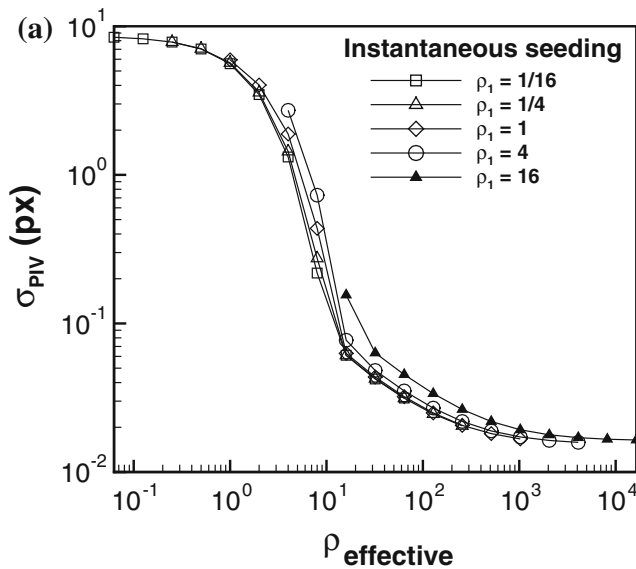


Fig. 3 Standard deviation of PIV error (px) as a function of increasing number of correlation averages, N . **a** Varying instantaneous seeding density, ρ_1 . The error is plotted against the effective seeding density, $\rho_{\text{effective}}$, where $\rho_{\text{effective}} = \rho_1 \times N$. The image noise ratio, E_n , is 0.5%

and no post-interrogation vector validation is employed. **b** Varying image noise, E_n . The instantaneous seeding density is low ($\rho_1 = \frac{1}{16}$). The error with correlation averaging increases with increasing image noise

seeding densities, ρ_1 . Increasing $\rho_{\text{effective}}$ corresponds directly to increasing the number of correlation averages, N , as demonstrated by Eq. 2. In Fig. 3a, excellent collapse of data is achieved by plotting the data as a function of the effective seeding density. Increasing the effective seeding density increases the signal strength of the averaged cross-correlation map resulting in significant reductions in error. In cases of correlation maps with a low SNR, peak detection is optimised with the use of correlation averaging (Meinhart et al. 2000). A secondary trend can also be seen in Fig. 3a: in general, at any effective seeding density, lower errors occur when lower instantaneous seeding densities are used in conjunction with correlation averaging. These higher signal-to-noise ratios are the result of smaller number of false correlations.

Figure 3b demonstrates the effect of increasing image noise on σ_{PIV} . The relative increase in error is minor for low levels of image noise which is consistent with the work on image noise and quantisation levels by Raffel et al. (2007) and Willert (1996). However, increasing the number of correlation averages, N , becomes less effective with

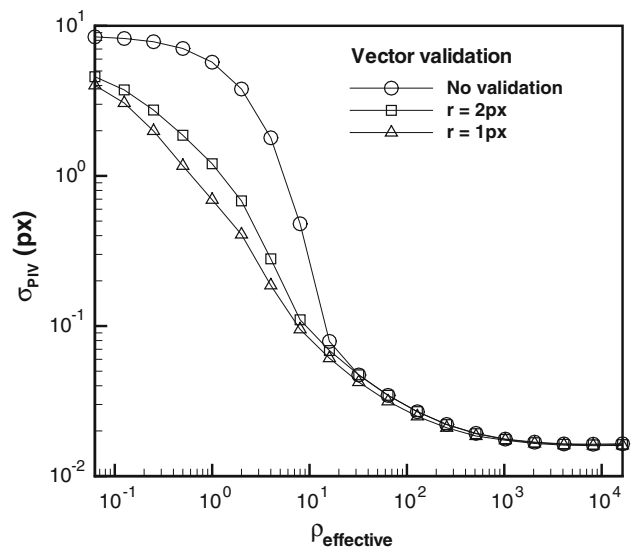


Fig. 4 Standard deviation of the PIV error as a function of effective seeding for different vector validation thresholds, r . Results are shown for images with a low instantaneous seeding density ($\rho_1 = \frac{1}{16}$), and low image noise ($E_n = 0.5\%$)

increasing image noise. More correlation averages are required to average the noise artefacts in the cross-correlation map.

Figure 4 shows the effect of vector validation on σ_{PIV} as the number of correlation averages is increased. Vector validation greatly enhances the accuracy of correlation averaging at lower effective seeding densities since the low seeding contributes to a poor correlation map and higher number of outliers. As the number of correlation averages is increased, vector validation has little effect on the measurement accuracy. The vector validation algorithm used in this analysis is a median level vector validation technique (Westerweel 1994) where r is the validation threshold (in pixels). Details of vector validation algorithms are not discussed here as this work has been covered in detail by Westerweel and Scarano (2005). For larger $\rho_{\text{effective}}$, the error in Fig. 3 converges to approximately 0.01 px. This limit has been observed with the 3-point parabolic fit we have used, in previous literature (Willert and Gharib 1991).

Correlation averaging is ideally suitable for images with low instantaneous seeding as the algorithm improves the correlation map signal by increasing the effective seeding density in the sampling window. This is consistent with the work of Meinhart et al. (1999, 2000), where correlation averaging yielded optimal results with approximately $N = 20$ correlation averages. Our analysis also confirms that improving the signal via correlation averaging is effective; however, this trend diminishes with increasing image noise. Vector averaging is an effective algorithm if the signal strength of the instantaneous correlation maps is

adequate. The accuracy of vector averaging is dependent on the quality of the vectors averaged; therefore, vector validation improves the measurement reliability (Fig. 2b).

In summary, correlation averaging enhances peak strength and reduces the percentage of outliers selected during peak detection by increasing the effective seeding density within a sampling window. However, improvements to the shape of the peak through correlation averaging, and hence optimisation to peak interpolation, are inefficient compared to vector averaging. Vector averaging reduces the measurement standard deviation with increasing number of averages. However, the measurement accuracy of vector averaging is dependent on the percentage of outliers present. The authors propose a new algorithm, hybrid averaging, which uses correlation averaging followed by vector averaging to obtain time-averaged measurements; such that both processes in PIV interrogation are optimised.

3 A hybrid averaging technique

A hybrid averaging process that utilises both correlation and vector averaging algorithms is proposed. The new algorithm, illustrated in Fig. 5, involves splitting the image sequence of M image pairs, into Q subsets of N image pairs. N image pairs are correlation averaged to get Q averaged displacement measurements. A vector average of Q measurements yields the time-averaged displacement measurement.

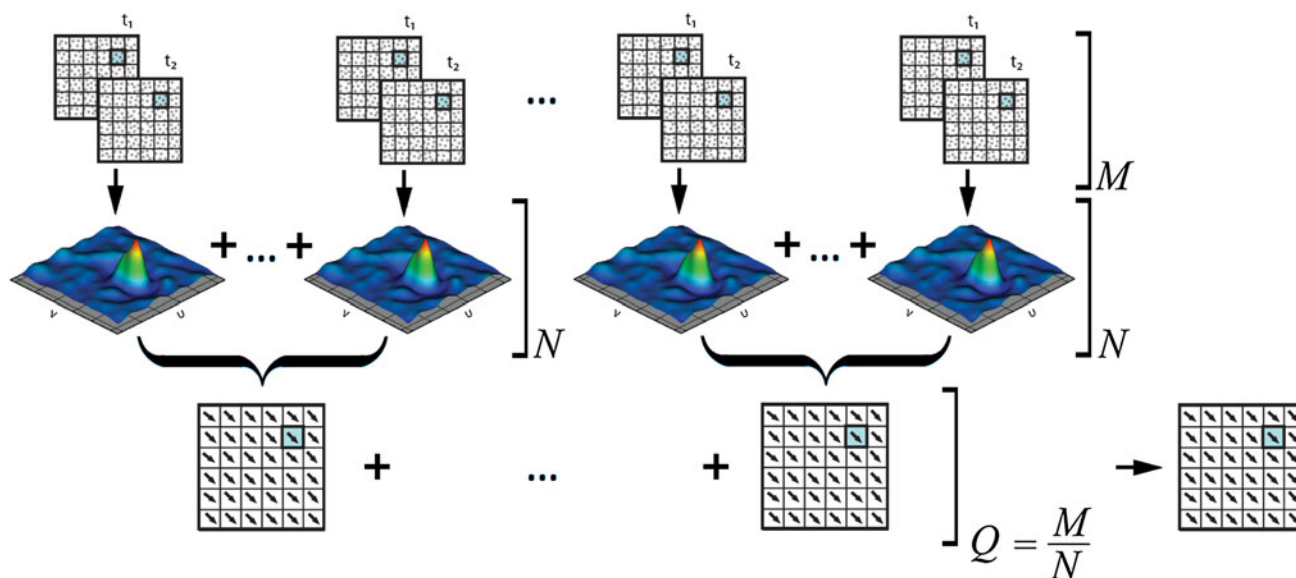


Fig. 5 Schematic of the hybrid averaging algorithm that uses an amalgamation of vector averaging and correlation averaging, N . Instantaneous correlation maps are correlation averaged to yield Q averaged correlation maps. The vectors from the averaged cross-

correlation map are vector averaged to obtain the time-averaged measurement. When the number of pairs in a correlation average, N , is 1, hybrid averaging represents vector averaging. Likewise, $N = M$ represents correlation averaging

To optimise the hybrid averaging algorithm, the number of pairs in a correlation average, N , is varied thus altering the ratio of correlation averaging to vector averaging, where this ratio represents the relative optimisation for either peak detection or peak interpolation. When $N = 1$, the hybrid averaging algorithm simply represents vector averaging. However with $N = M$, the algorithm averages all instantaneous correlation map to yield one averaged correlation map, representing correlation averaging. Clearly, the interesting region of parameter space is when $1 < N < M$, where the algorithm uses a hybrid ratio of correlation averaging to vector averaging to obtain displacement measurements.

To test the new algorithm, synthetic image pairs for a low spatial gradient flow (Table 1: C) were generated. The data set consisted of 1,024 image pairs (M). The image noise ratio E_n was varied from 0.5% to 50.0%. PIV data sets for another flow type with a high spatial gradient (Table 1: A) were tested with the results following similar trends, and for brevity, these results are not discussed. Other parameters used for generating the images are equivalent to the parameters discussed in Sect. 2.2.

Results for a low noise (0.5%) and a high noise (50%) data set are shown. The error statistics are determined for each case of hybrid averaging for the different instantaneous seeding densities and image noise ratios. Figure 6 shows a plot of the relative accuracy for low noise images

($E_n = 0.5\%$) with low seeding ($\rho_1 = \frac{1}{16}$) using hybrid averaging. The relative accuracy is the difference in the PIV error obtained through hybrid averaging (σ_{PIV}) compared to the PIV error with correlation averaging ($(\sigma_{PIV})_c$), expressed as a percentage, as shown in Eq. 3. Thus, positive values of relative accuracy represent an improvement in the PIV error relative to correlation averaging. The relative accuracy is plotted as a function of both the effective seeding density and the number of pairs in a correlation average, N , where as discussed previously the increase in N corresponds to an increase in the effective seeding density.

$$\text{Relative accuracy (\%)} = \frac{(\sigma_{PIV})_c - \sigma_{PIV}}{(\sigma_{PIV})_c} \times 100 \quad (3)$$

3.1 Low image noise

Figure 7a shows the relative accuracy as a function of N for low noise images with instantaneous seeding densities ranging from $\frac{1}{16}$ to 16 ppw. The simulations show that at very low instantaneous seeding densities ($\frac{1}{16} \leq \rho_1 \leq 1$), correlation averaging ($N = 1,024$) has superior measurement accuracy over vector averaging ($N = 1$), which is consistent with previous findings (Meinhart et al. 2000; Wereley and Meinhart 2010). However, optimised hybrid averaging yields a further improvement of 4% compared to correlation averaging for the low instantaneous seeding density cases ($\frac{1}{16} \leq \rho_1 \leq 1$). When the seeding density is low, increasing amounts of correlation averaging help optimise the peak detection error. By subsequently performing vector averaging with hybrid averaging, the peak interpolation error is further optimised.

When the instantaneous seeding density is high ($\rho_1 \geq 4$), the PIV error is reduced by vector averaging ($N = 1$). When there are an adequate number of particles in a sampling window (Keane and Adrian 1992), no further optimisation is gained through correlation averaging. The relative accuracy of vector averaging over correlation averaging for $\rho_1 = 4$ is around 4%. However, with increasing instantaneous seeding density, the relative benefits of vector averaging over correlation averaging diminish to 2% for $\rho_1 = 16$. Figure 7b shows the data plotted in Fig. 7a replotted as a function of the effective seeding density. The excellent collapse of the data points illustrates that relative accuracy is strongly dependent on the effective seeding density. The relative accuracy is optimised when the effective seeding density is around seven particles per window. This is in agreement with a previous study (Keane and Adrian 1992), which recommends at least seven particle image pairs in a sampling window for an ideal correlation.

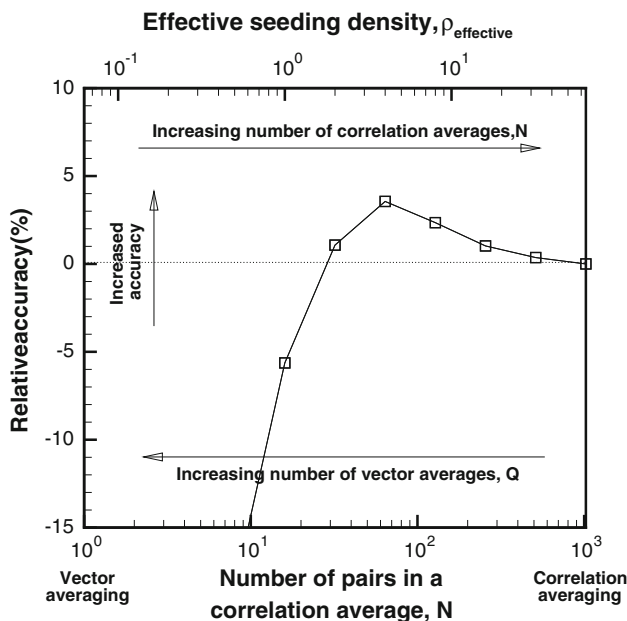


Fig. 6 Relative accuracy (percentage relative to correlation averaging) as a function of increasing number of pairs in a correlation average, N , and the effective seeding density. The image series has a low seeding density ($\rho_1 = \frac{1}{16}$), low image noise ($E_n = 0.5\%$) and 1,024 image pairs. The number of pairs in a correlation average, N , is varied from 1 (vector averaging) to 1,024 (correlation averaging)

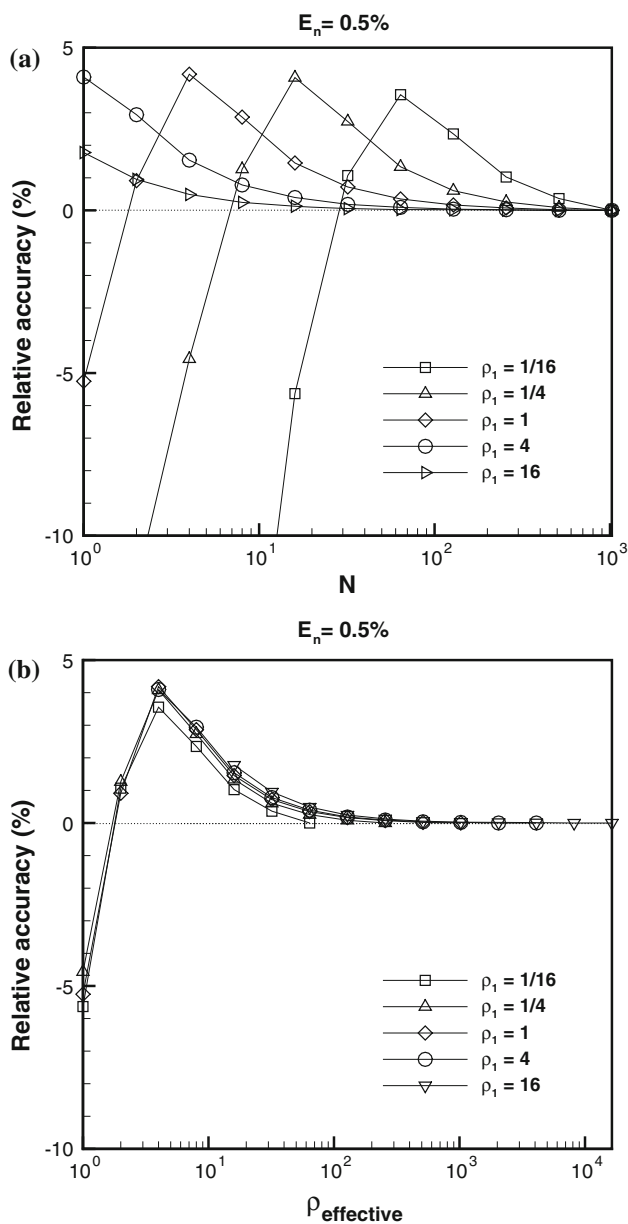


Fig. 7 Hybrid averaging with low image noise. **a** Relative accuracy as a function of increasing number of correlation averages, N , for images with low noise ($E_n = 0.5\%$). For low and moderate instantaneous seeding ($\frac{1}{16} \leq \rho_1 \leq 1$), the relative accuracy is improved at intermediate values of N corresponding to hybrid averaging. For high seeding densities ($\rho_1 \geq 4$), vector averaging optimises the PIV error. **b** The same data are now plotted as a function of the effective seeding density, $\rho_{\text{effective}}$. Excellent collapse of the data points is evident with the optimal effective seeding density being approximately seven particles per sampling window

3.2 High image noise

Figure 8a shows the relative accuracy for hybrid averaging plotted as a function of N for high noise images with instantaneous seeding densities ranging from 1 to 16 ppw. For these high noise cases, only seeding densities of $\rho_1 \geq 1$

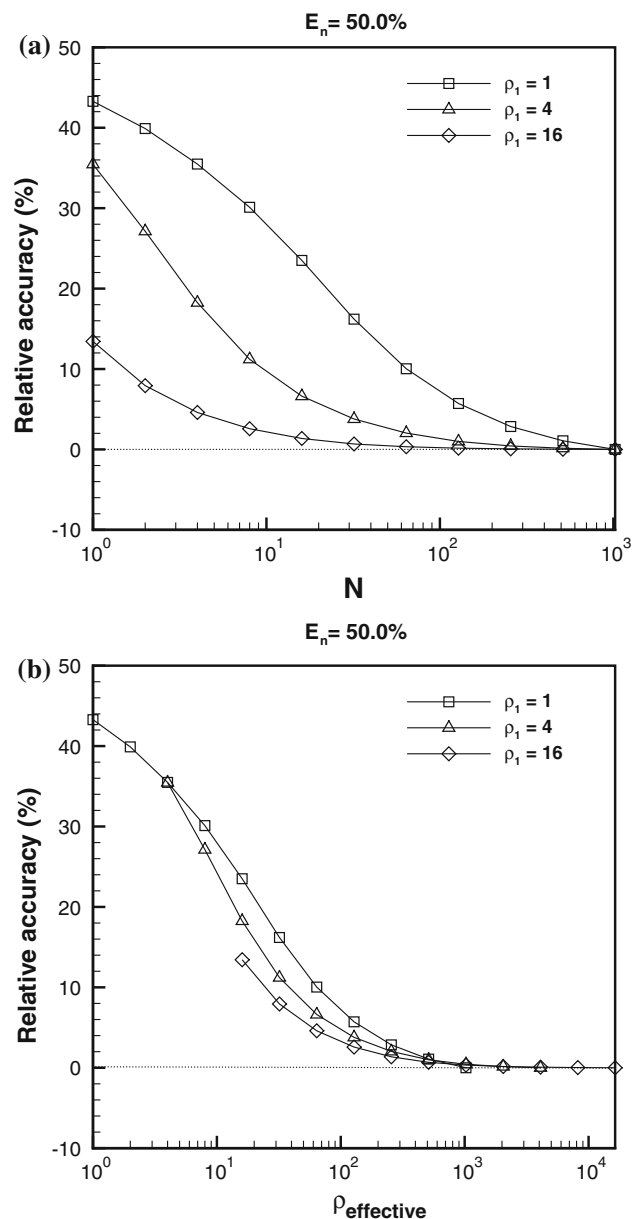


Fig. 8 Hybrid averaging with high image noise. **a** Relative accuracy as a function of increasing number of correlation averages, N , for images with high image noise ($E_n = 50.0\%$). For cases of moderate to high instantaneous seeding ($\rho_1 \geq 1$), vector averaging yields the most optimal measurement accuracy over correlation averaging (at least 40%). **b** The same data are now plotted as a function of the effective seeding density, $\rho_{\text{effective}}$. The data points do not collapse as well as those observed in the low image noise case (Fig. 7b)

produce satisfactory conditions for acceptable PIV measurements. For moderate to high seeding densities ($\rho_1 \geq 1$), vector averaging improves the relative PIV accuracy over correlation averaging. Vector averaging ($N = 1$) yields superior measurement accuracy with improvements in the relative accuracy of up to 40% compared to correlation averaging. The results from Fig. 8a are plotted as a function of the effective seeding density in

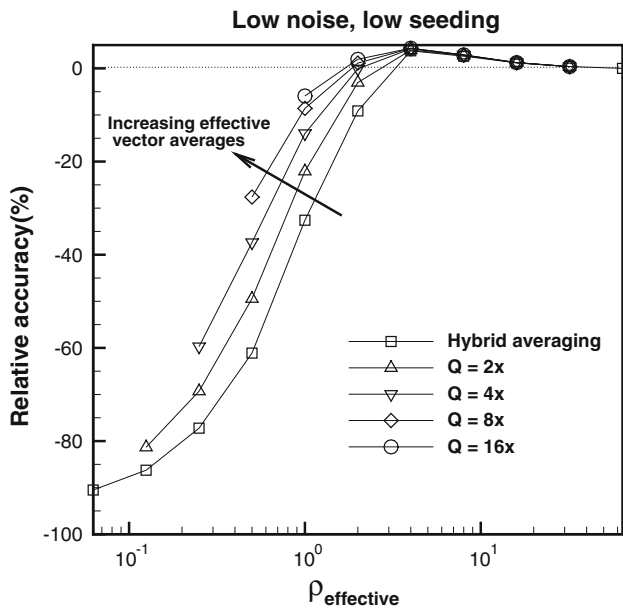


Fig. 9 Relative accuracy of hybrid averaging with temporal image oversampling. Temporal image oversampling involves reusing image pairs in an image sequence to increase the number of vector averages in a hybrid average. The images used in this simulation have low instantaneous seeding density and low image noise. Improvements of measurement accuracy are evident with increasing image oversampling. Temporal image oversampling only improves sub-optimal cases when the effective seeding density is low

Fig. 8b. Collapse of the data points indicates a dependence on the effective seeding density; however, the collapse is not as tight as for the low noise cases.

3.3 Image oversampling

Image oversampling is a process by which image pairs in a given sequence of images are oversampled, thereby increasing the number of vector averages in a hybrid average. Figure 9 shows the relative accuracy as a function of the effective seeding density for hybrid averaging with and without temporal image oversampling. The different curves represent increasing amounts of oversampling that increases the number of vector averages by two to sixteen times. The images used have low seeding and low image noise. Increasing oversampling reduces the PIV error for sub-optimal effective seeding densities. This was confirmed with highly seeded images where temporal image oversampling made no improvement over hybrid averaging.

4 Recommendations: steady flows

We have established the mechanisms by which vector averaging and correlation averaging improve measurement accuracy. Vector averaging optimises by improving peak

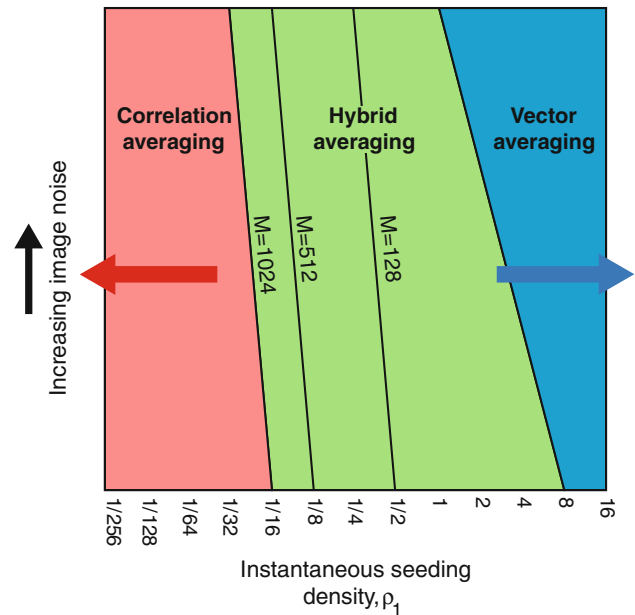


Fig. 10 Regimes for the optimal temporal averaging process. The regimes are defined as a function of the instantaneous seeding density and image noise. Correlation averaging is optimal when a data set has a low seeding density or when there are fewer frames. If the seeding density is above 7 particles per window, regardless of image noise, vector averaging is the recommended process. For a regime of parameter space in between the above-mentioned regimes, the novel hybrid averaging process is the most accurate

interpolation and correlation averaging by optimising peak detection. Based on this, we have proposed a new hybrid averaging process that utilises both vector and correlation averaging. Below are summarised a few recommendations in determining the optimal averaging process.

We define three regimes, as shown in Fig. 10, to help explain these recommendations. These regimes are defined as a function of the instantaneous seeding density and image noise.

1. In cases of low image seeding, i.e. when $\rho_{\text{effective}} < 7$ or $\rho_1 < \frac{7}{M}$, it is recommended to use correlation averaging alone. The low image seeding results in a poor signal to noise ratio decreasing the detectability of the signal peak.
2. In cases where there are 7 or more particle image pairs in a sampling window (Keane and Adrian 1992), no further optimisation is measurement accuracy is achieved by optimising for peak detection (correlation averaging). In this regime, it is recommended to use vector averaging to determine the averaged velocity field.
3. In cases of moderate seeding density, i.e. when $\frac{7}{M} < \rho_1 \leq 8$, hybrid averaging delivers the highest measurement accuracy. Hybrid averaging is the most accurate process when there is an effective seeding of 7 particles per window ($\rho_{\text{effective}} = 7$).

4. Decreasing the size of the data set, M , favours correlation averaging as the optimal process. This is denoted by the lines in Fig. 10. Increasing the size of the data set favours additional vector averages as the chances of achieving the optimal effective seeding density of 7 ppw are higher.
5. If the images have high levels of noise and moderate to high levels of seeding, then it is recommended that vector averaging is used. PIV measurements in cases of high image noise and low seeding are not recommended; however, depending on how many frames are included in the average, hybrid averaging or correlation averaging could be employed.
6. Temporal image oversampling is beneficial to improve averaging accuracy if the seeding density is inadequate for hybrid averaging.
7. Consider the use of the sampling window size to obtain further improvements in measurement accuracy when using hybrid averaging. In this way, one can vary the seeding density in a sampling window by varying the window size.

5 Application to experimental data

5.1 Application to micro-PIV

Hybrid averaging was applied to two different sets of experimental images, a μ PIV flow inside a model of a stenosis; and a traditional PIV flow behind a circular cylinder.

A glycerol solution (50% Water/Glycerol) was seeded with 6- μ m fluorescent particles (0.075% solids). The model of the stenosis is 200 μ m \times 6,000 μ m, while the stenosed section is 3,000 μ m wide. The flow was set at a flow rate of $V = 0.48$ ml/min, using the hydrostatic pressure differential, Δh , between the fluid levels in the inlet and outlet reservoirs and verified using a flowmeter (Transonic TS420). The centre of the micro-channel is illuminated using a continuous diode-pumped solid-state laser source (Melles Griot, Wavelength = 532 nm) as shown in Fig. 11. 1,000 image pairs of the flow were captured using a high speed digital camera at a rate of 200 fps (IDT Y4, 1,016 \times 1,016 px²) through a 5 \times NA = 0.15 objective lens (Leica).

A subset of 512 image pairs was evaluated using hybrid averaging. The number of image pairs in a correlation average, N , was varied from $N = 1$ (vector averaging) to $N = 512$ (correlation averaging). Figure 12 shows the averaged velocity field of the complex flow through the micro-channel, evaluated with hybrid averaging ($N = 4$).

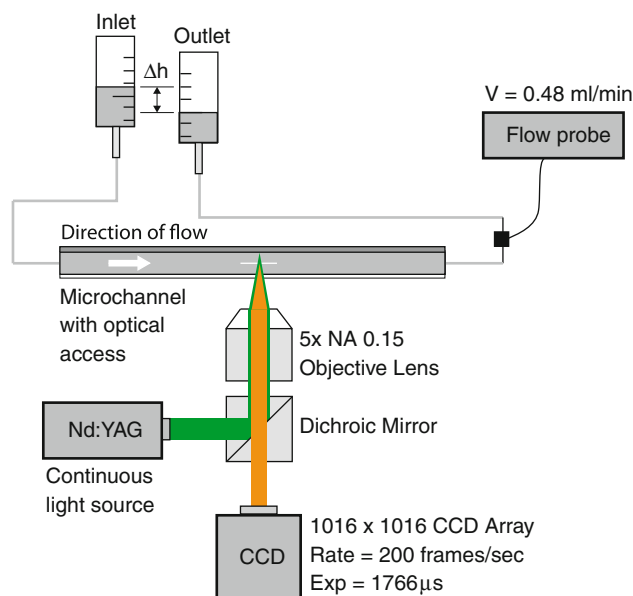


Fig. 11 Experimental set-up used for the μ PIV experiments. The micro-channel is a complete model of a stenosis, and the flow has a low Reynolds number ($Re \ll 1$)

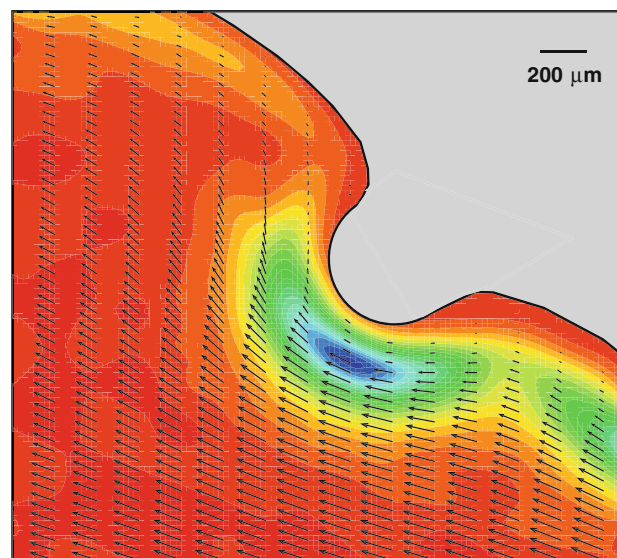


Fig. 12 Hybrid-averaged velocity (vectors) and vorticity field (contours) for the μ PIV experiment (Table 1: E). The number of correlation averages in a pair was 4 image pairs ($N = 4$). Only every 8th vector in x and 2nd vector in y are shown for the purpose of clarity

The contours represent the vorticity field where the vorticity is calculated using the method specified by Fouras and Soria (1998).

Typically, a standard method to determine the averaged displacement would be to correlation average the image pairs. In our case, we correlation averaged 1,000 image pairs and assumed this to be the correct result. The relative PIV error, i.e. the difference in the PIV error between the

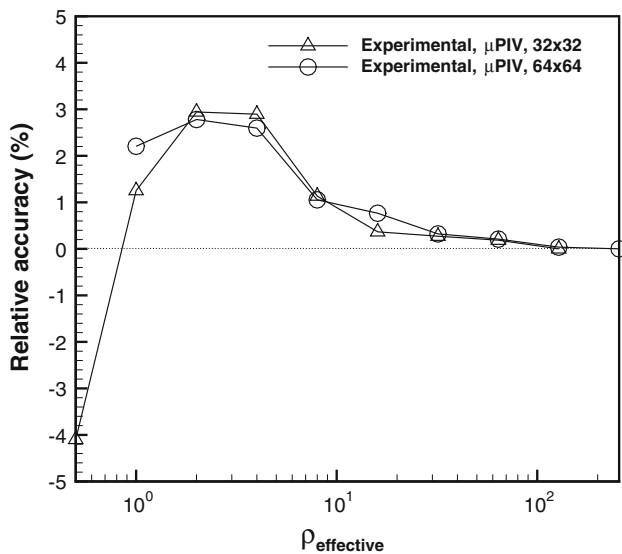


Fig. 13 Relative accuracy as a function of the effective seeding density for evaluating the averaged measurements of the μ PIV flow, with different sampling window sizes. The evident collapse of the data points when plotted as a function of the effective seeding density is similar to that found in the low image noise cases of the Monte Carlo simulation (Fig. 7b)

hybrid-averaged measurement and the standard correlation-averaged measurement ($N = 1,000$), was determined for each value of N . The relative accuracy of the PIV error was calculated using Eq. 3. The image sequences were analysed separately using different sampling window sizes, W (recommendation 7). Figure 13 shows the relative accuracy of hybrid averaging versus the effective seeding density for two sampling window sizes. Optimised hybrid averaging ($N = 4$) is approx. 3% more accurate than correlation averaging, irrespective of window size. The collapse of the relative accuracy as a function of $\rho_{\text{effective}}$ is similar to that observed in the low noise theoretical simulations (Fig. 7b).

To simulate images with high sensor noise, synthetic noise with a Poisson distribution was added to the μ PIV image sequence. In similar fashion to the high noise theoretical simulations carried out in Sect. 3, vector averaging ($N = 1$) improved the measurement accuracy by 86% (not shown) over standard correlation averaging.

5.2 Application to macro-PIV

The hybrid averaging process was further evaluated via the application of macro-PIV to the steady wake behind a circular cylinder. The circular cylinder, placed in a shallow water table, was used for the simultaneous measurement of the velocity field and the surface topography (Ng et al. 2011; Fouras et al. 2008).

The wake is steady at a Reynolds number (Re) of 66; however, since the cylinder is at a shallow depth, the flow

cannot be directly compared to a fully submerged cylinder wake. The three temporal averaging processes, vector, correlation and the novel hybrid averaging process, were applied to determine the averaged velocity and vorticity fields. The sampling window size was 32×32 pixels², corresponding to an average instantaneous seeding density of 1–2 particles per window. The image sequence has low image noise and consists of 512 image pairs.

Figure 14 shows the averaged measurements evaluated using the three temporal averaging processes. The vectors represent the averaged velocity, while the contours represent the vorticity. As indicated by the smoothness of the vorticity contours (Fig. 14b), hybrid averaging delivers superior measurement accuracy over vector averaging (Fig. 14a), and a subtly more accurate measurement over correlation averaging (Fig. 14c). This is in close agreement with the results from the Monte Carlo simulations described in Sect. 3 and the recommendations in Fig. 10, for $\rho_1 = 1$ ppw and low image noise. Hybrid averaging optimised when $N = 8$, which corresponds to an effective seeding density of 7 or more particles per window (Keane and Adrian 1992).

6 Application to transient flows

6.1 Synthetic Monte Carlo simulation

Correlation averaging has become the standard time-averaging process for various applications of PIV and is preferred in conditions with low seeding and high noise (Wereley and Meinhart 2010). However, under some experimental conditions, such as those found in biological flows, the flow is not always steady. Although correlation averaging improves the signal to noise ratio to yield improved measurements in these conditions (Meinhart et al. 2000), the transient nature of the flow can lead to spurious results (Poelma et al. 2010).

Figure 15 shows the effect of using correlation averaging on pulsatile flow measurements. The averaged cross-correlation function is bimodal due to the transient flow conditions (Fig. 15a). The resulting displacement measurements are then biased towards either of the maxima and never towards the mean signal. The signal peak closest to zero is preferred as evident on the biased displacement measurements shown in Fig. 15b. Recently, Poelma and Westerweel (2010) showed that in cases with time-varying flow, conventional peak fitting methods are not recommended.

Here, we conduct a Monte Carlo simulation to study the application of current time-averaging processes and hybrid averaging to pulsatile conditions. Synthetic images were generated as outlined in Sect. 2.2. The images are based on a simple oscillatory flow (Eqs. 4, 5) and have low image

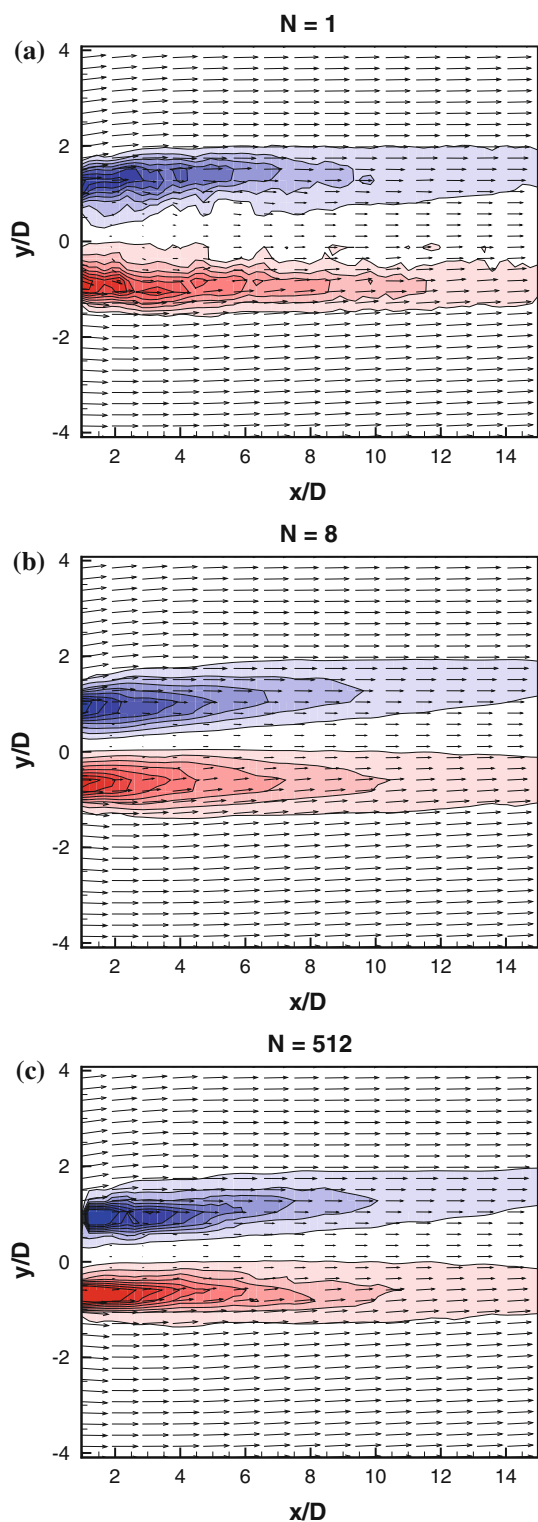


Fig. 14 Averaged velocity (vectors) and vorticity (contours) of the flow behind a cylinder at $Re = 66$. The averaged measurements were evaluated using (a) vector averaging; (b) hybrid averaging; and (c) correlation averaging. Hybrid averaging with 8 image pairs in a correlation average ($N = 8$), yields the optimal measurement accuracy over vector averaging and correlation averaging

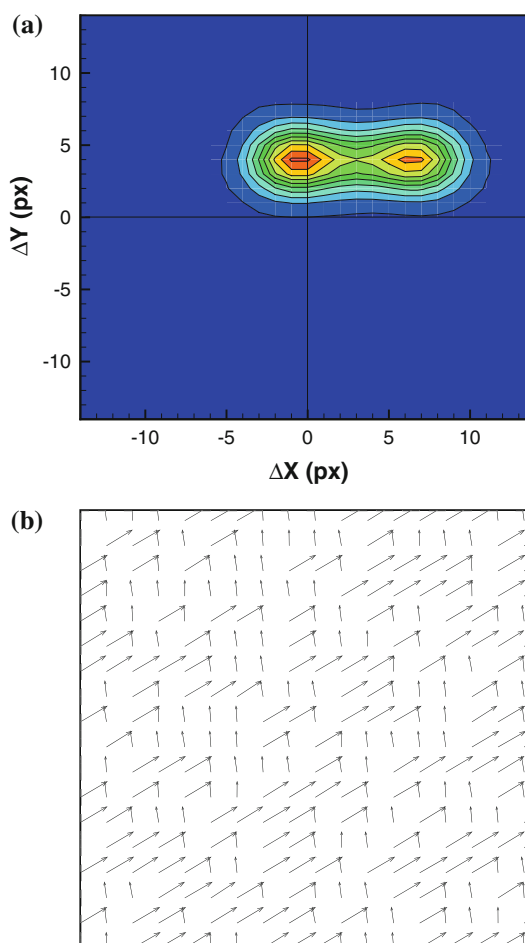


Fig. 15 Effect of correlation averaging in transient flows. **a** Contours of the averaged cross-correlation function for a time-varying flow (Eqs. 4, 5). The PDF is bimodal in nature with two distinct maxima for the PIV signal. The amplitude of the sinusoid is 5 px. **b** The resulting averaged displacement field from evaluating the averaged cross-correlation function. The displacement measurement is biased towards either one of the bimodal maxima from the averaged cross-correlation function depending on random noise and never selects the average value

noise ($E_n = 0.5\%$). The oscillatory flow has an amplitude of 5 pixels, and the entire image sequence has two time periods of the oscillation. In this particular case, the flow follows Eqs. 4 and 5.

$$u = 3.0 + 5\cos(\omega t) \quad (4)$$

$$v = 4.0 \quad (5)$$

Figure 16 shows the relative accuracy (Eq. 3) as a function of N , for instantaneous seeding densities varying from $\frac{1}{16}$ to 16 particle per window. N was varied from $N = 1$ (vector averaging) to $N = 1,024$ (correlation averaging). The gains in the measurement accuracy over correlation averaging ($N = 1,024$) of both hybrid and vector averaging

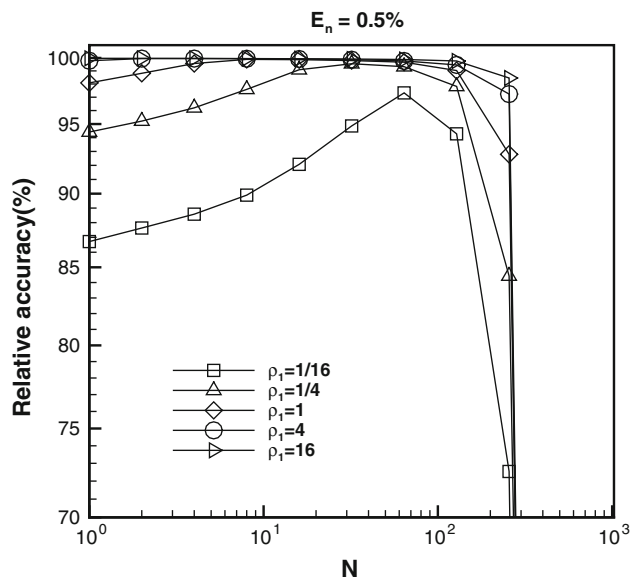


Fig. 16 Relative accuracy plotted against the number of image pairs in a correlation average, N , for different synthetic image sequences of varying instantaneous seeding density, ρ_1 . For cases when $\rho_1 \leq 1$, hybrid averaging improves the measurement accuracy over current averaging processes. For images with high seeding density ($\rho_1 \geq 4$), vector averaging is the optimal averaging process, while hybrid averaging offers similar accuracy. The time variant nature of the flow decreases the measurement accuracy of correlation averaging. Hence, hybrid averaging offers improved accuracy (96–98%) over correlation averaging

are immense due to the biased measurements resulting from the summation of the instantaneous cross-correlations. For images with low seeding density ($\rho_1 < 1$), hybrid averaging yields in superior measurement accuracies over vector averaging (10–80%) and immense accuracy over correlation averaging (96–98%).¹ As the number of particles in a sampling window increases ($\rho_1 \geq 4$), vector averaging provides excellent accuracy over correlation averaging. However, the accuracy of hybrid averaging is as accurate as that of vector averaging. In cases with lower seeding densities, phase averaging may be suitable but are limited by the number of averages. The optimal measurement is still dependent on the instantaneous seeding density and the number of correlation averages (optimise peak detection) and the number of vector averages (optimise peak interpolation).

6.2 Application to an unsteady wake behind a circular cylinder

Hybrid averaging was applied to an unsteady wake behind a circular cylinder. The experimental conditions are similar to that used in Sect. 5.2. The cylinder is placed in shallow

¹ Relative accuracy of the PIV error from hybrid averaging to the PIV error from vector averaging.

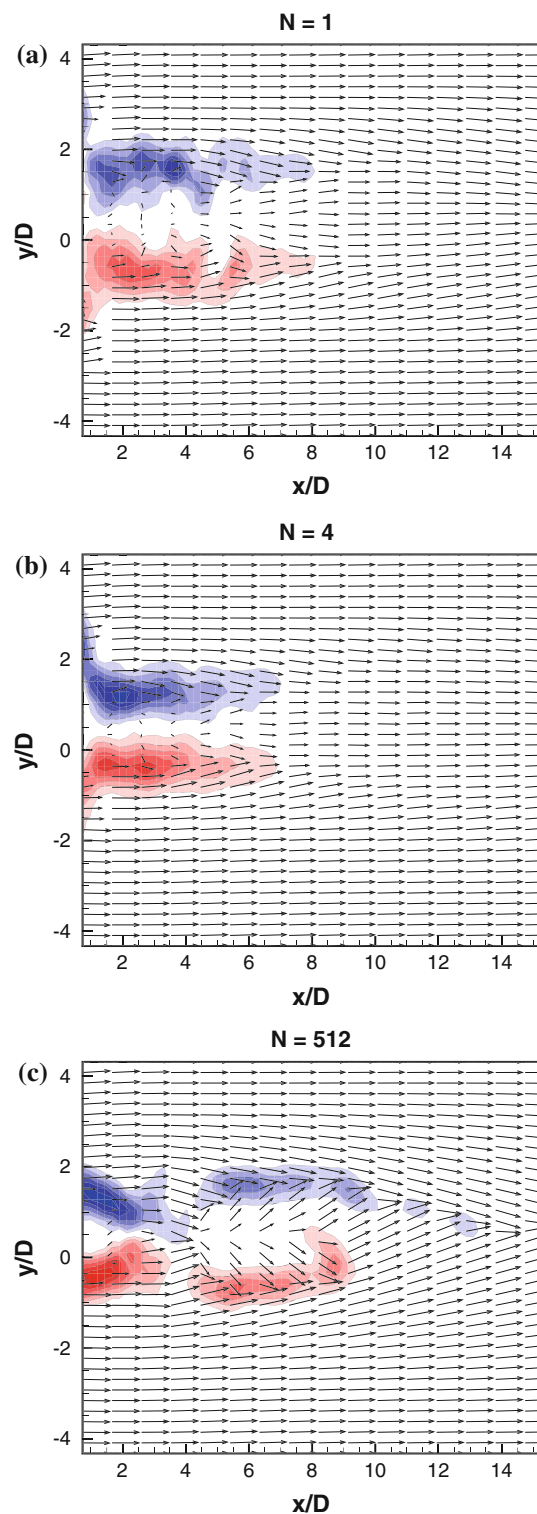


Fig. 17 Averaged velocity (vectors) and vorticity (contours) of the flow behind a cylinder at $Re = 98$. The averaged measurements were evaluated using (a) vector averaging; (b) hybrid averaging; and (c) correlation averaging. The sinusoidal nature of the wake behind the cylinder greatly deteriorates the measurement accuracy of correlation averaging. Hybrid averaging yields optimal averaging accuracy over vector averaging and correlation averaging, as is clearly represented by the vorticity contours

water with flow of Reynolds number, $Re = 98$. The size of the sampling window size was $64 \times 64 \text{ pixel}^2$, and the flow seeding conditions were similar to the steady flow case in Sect. 5.2. The data set comprised of 512 image pairs. For further reference to experimental conditions, please refer to the recent work by Ng et al. (2011).

Figure 17 shows the averaged velocity vectors with contours for vorticity obtained by vector, hybrid and correlation averaging. Correlation averaging ($N = 512$) yields averaged measurements biased by the pulsatile nature of the wake. Vector averaging ($N = 1$) yields averaged measurements more accurate than correlation averaging. However, due to inadequate seeding ($\rho_1 = 4$), the contours for vorticity are not as well defined (Fig. 17a) as those obtained from hybrid averaging. Hybrid averaging with 4 image pairs in a correlation average ($N = 4$) yielded the most accurate averaged measurement (Fig. 17b). The hybrid-averaged measurements are superior to correlation averaging as can be determined by the correct wake profile and smooth vorticity contours. This trend is similar to that observed in our synthetic simulations (Fig. 16) for an instantaneous seeding of 4 ppw with low image noise.

7 Summary and conclusions

We have introduced a novel hybrid averaging process which incorporates a combination of correlation and vector averaging processes. Correlation, vector and the novel hybrid averaging processes have been evaluated using an extensive series of Monte Carlo simulations and laboratory experiments. The simulations evaluated the averaging processes using synthetic images for both steady and pulsatile flow conditions; varying tracer seeding densities and image noise levels. The averaging techniques were applied to a flow in a stenosed micro-channel and the wake behind a circular cylinder. Comparisons between the measurement accuracy of hybrid averaging to that of vector averaging and correlation averaging showed that hybrid averaging is optimal over a wide range of imaging conditions.

Guidelines have been developed to select the optimal temporal averaging process for various seeding levels, image noise and flow conditions. In cases where there is an inadequate number of particles in a sampling window or a lower number of frames in the image sequence, correlation averaging is recommended. In cases with adequate seeding (7 or more particles in a sampling window), vector averaging is recommended. However, over a wide parameter space in between these two regimes, hybrid averaging yields the most accurate measurement. Hybrid averaging is optimised when there are sufficient correlation averages to achieve an effective seeding density of approximately 7 particles per window. For larger data sets, higher effective seeding can

allow smaller sampling window sizes to be used, resulting in a higher spatial resolution of the time-averaged measurement. For noisy images with moderate to high seeding densities (more than 1 particle per window), vector averaging gives a greater accuracy than correlation averaging.

Pulsatile flow provides additional challenges producing multi-modal correlation peaks, and the use of correlation averaging is not recommended. For pulsatile images with high seeding, i.e. 7 or more particle image pairs in a sampling window, vector averaging is recommended; in all other cases, hybrid averaging is the recommended temporal averaging process.

Acknowledgments A. F. acknowledges discussions with Dr. David Lo Jacono. The authors would like to acknowledge the support of Mr. Jordan Thurgood in conducting the experiments and Mr. Ivan Ng for the circular cylinder experimental image sequences. Support from the Australian Research Council under Discovery Grants DP0877327 and DP0987643 are gratefully acknowledged. C.R.S. is a recipient of an Australian Postgraduate Award.

References

- Adrian RJ (2005) Twenty years of particle image velocimetry. *Exp Fluids* 39:159–169
- Delnoji E, Westerweel J, Deen NG, Kuipers JAM, van Swaaij WPM (1999) Ensemble correlation piv applied to bubble plumes rising in a bubble column. *Chem Eng Sci* 54:5159–5171
- Dubsky S, Jamison RA, Irvine SC, Siu KKW, Hourigan K, Fouras A (2010) Computed tomographic x-ray velocimetry. *Appl Phys Lett* 96(023702):1–3
- Fouras A, Soria J (1998) Accuracy of out-of-plane vorticity measurements derived from in-plane velocity field data. *Exp Fluids* 25:409–430
- Fouras A, Dusting J, Lewis R, Hourigan K (2007) Three-dimensional synchrotron x-ray particle image velocimetry. *J Appl Phys* 102(064916)
- Fouras A, Jacono DL, Hourigan K (2008) Target-free stereo PIV: a novel technique with inherent error estimation and improved accuracy. *Exp Fluids* 44:317–329
- Fouras A, Jacono DL, Sheard GJ, Hourigan K (2008) Measurement of instantaneous velocity and surface topography in the wake of a cylinder at low Reynolds number. *J Fluid Struct* 24(8):1271–1277
- Fouras A, Jacono DL, Nguyen CV, Hourigan K (2009) Volumetric correlation PIV: a new technique for 3D velocity vector field measurement. *Exp Fluids* 47(4-5):569–577
- Hart DP (2000) PIV error correction. *Exp Fluids* 29(1):13–22
- Huang H, Dabiri D, Gharib M (1997) On errors of digital particle image velocimetry. *Meas Sci Technol* 8:1427–1440
- Irvine SC, Paganin DM, Dubsky S, Lewis RA, Fouras A (2008) Phase retrieval for improved 3d velocimetric analysis of X-ray blood flow speckle patterns. *Appl Phys Lett* 93(153901):1–3
- Keane RD, Adrian RJ (1990) Optimization of particle image velocimeters: I. double pulsed systems. *Meas Sci Technol* 1:1202–1215
- Keane RD, Adrian RJ (1992) Theory of cross-correlation analysis of PIV images. *Appl Sci Res* 49:191–215
- Landreth CC, Adrian RJ (1990) Impingement of a low Reynolds number turbulent circular jet onto a flat plate at normal incidence. *Exp Fluids* 9:74–84

- Lourenco LM, Krothapalli A (1995) On the accuracy of velocity and vorticity measurements with PIV. *Exp Fluids* 18(6):421–428
- Meinhart CD, Wereley ST, Santiago JG (1999) PIV measurements of a microchannel flow. *Exp Fluids* 27(5):414–419
- Meinhart CD, Wereley ST, Santiago JG (2000) A PIV algorithm for estimating time-averaged velocity fields. *J Fluid Eng* 122(2):285–289
- Nesbitt WS, Westein E, Tovar-Lopez FJ, Tolouei E, Mitchell A, Fu J, Carberry J, Fouras A, Jackson SP (2009) A shear gradient-dependent platelet aggregation mechanism drives thrombus formation. *Nat Med* 15(6):665–673
- Ng I, Kumar V, Sheard GJ, Hourigan K, Fouras A (2011) Experimental study of simultaneous measurement of velocity and surface topography: in the wake of a circular cylinder at low Reynolds number. *Exp Fluids* 50:587–595
- Nguyen CV, Fouras A, Carberry J (2010) Improvement of measurement accuracy in micro-PIV by image overlapping. *Exp Fluids* 49:701–712
- Olsen MG, Adrian RJ (2000) Out-of-focus effects on particle image visibility and correlation in microscopic particle image velocimetry. *Exp Fluids* 29(7):S166–S174
- Olsen MG, Adrian RJ (2000) Brownian motion and correlation in particle image velocimetry. *Opt Laser Technol* 32:621–627
- Poelma C, Westerweel J (2010) Generalized displacement estimation for averages of non-stationary flows. *Exp Fluids* (Online)
- Poelma C, der Heiden KV, Hierck BP, Poelmann RE, Westerweel J (2010) Measurements of the wall shear stress distribution in the outflow tract of an embryonic chicken heart. *J R Soc Interface* 7-42:91–103
- Raffel M, Willert CE, Wereley ST, Kompenhans J (2007) Particle image velocimetry: a practical guide, 2nd edn. Springer, Berlin
- Roesgen T (2003) Optimal subpixel interpolation in particle image velocimetry. *Exp Fluids* 35(3):252–256
- Santiago JG, Wereley ST, Meinhart CD, Beebe DJ, Adrian RJ (1998) A particle image velocimetry system for microfluidics. *Exp Fluids* 25(4):316–319
- Theunissen R, Scarano F, Riethmuller ML (2007) An adaptive sampling and windowing interrogation method in PIV. *Meas Sci Technol* 18:275–287
- Theunissen R, Scarano F, Riethmuller ML (2010) Spatially adaptive piv interrogation based on data ensemble. *Exp Fluids* 48(5):875–887
- Tiang J, Qui H (2002) Eliminating background noise effect in microscopic particle image velocimetry. *Appl. Opt.* 41(32):6849–6857
- Wereley ST, Meinhart CD (2010) Recent advances in micro-particle image velocimetry. *Ann Rev Fluid Mech* 42:557–576
- Wereley ST, Gui L, Meinhart CD (2002) Advanced algorithms for microscale particle image velocimetry. *AIAA J* 40(6):1047–1055
- Westerweel J (1994) Efficient detection of spurious vectors in particle image velocimetry data. *Exp Fluids* 16(3):236–247
- Westerweel J (1997) Fundamentals of digital particle image velocimetry. *Meas Sci Technol* 8(12):1379–1392
- Westerweel J (2000) Theoretical analysis of the measurement precision in particle image velocimetry. *Exp Fluids* 29(7):3–12
- Westerweel J, Scarano F (2005) Universal outlier detection for PIV data. *Exp Fluids* 39(6):1096–1100
- Westerweel J, Geelhoed PF, Lindken R (2004) Single-pixel resolution ensemble correlation for micro-PIV applications. *Exp Fluids* 37(3):375–384
- Willert CE (1996) The fully digital evaluation of photographic PIV recordings. *Appl Sci Res* 56(2):79–102
- Willert CE, Gharib M (1991) Digital particle image velocimetry. *Exp Fluids* 10(4):181–193